Volume 12
Number 18
14 May 2024
Pages 6361–6704

Journal of Materials Chemistry C

Materials for optical, magnetic and electronic devices

rsc.li/materials-c

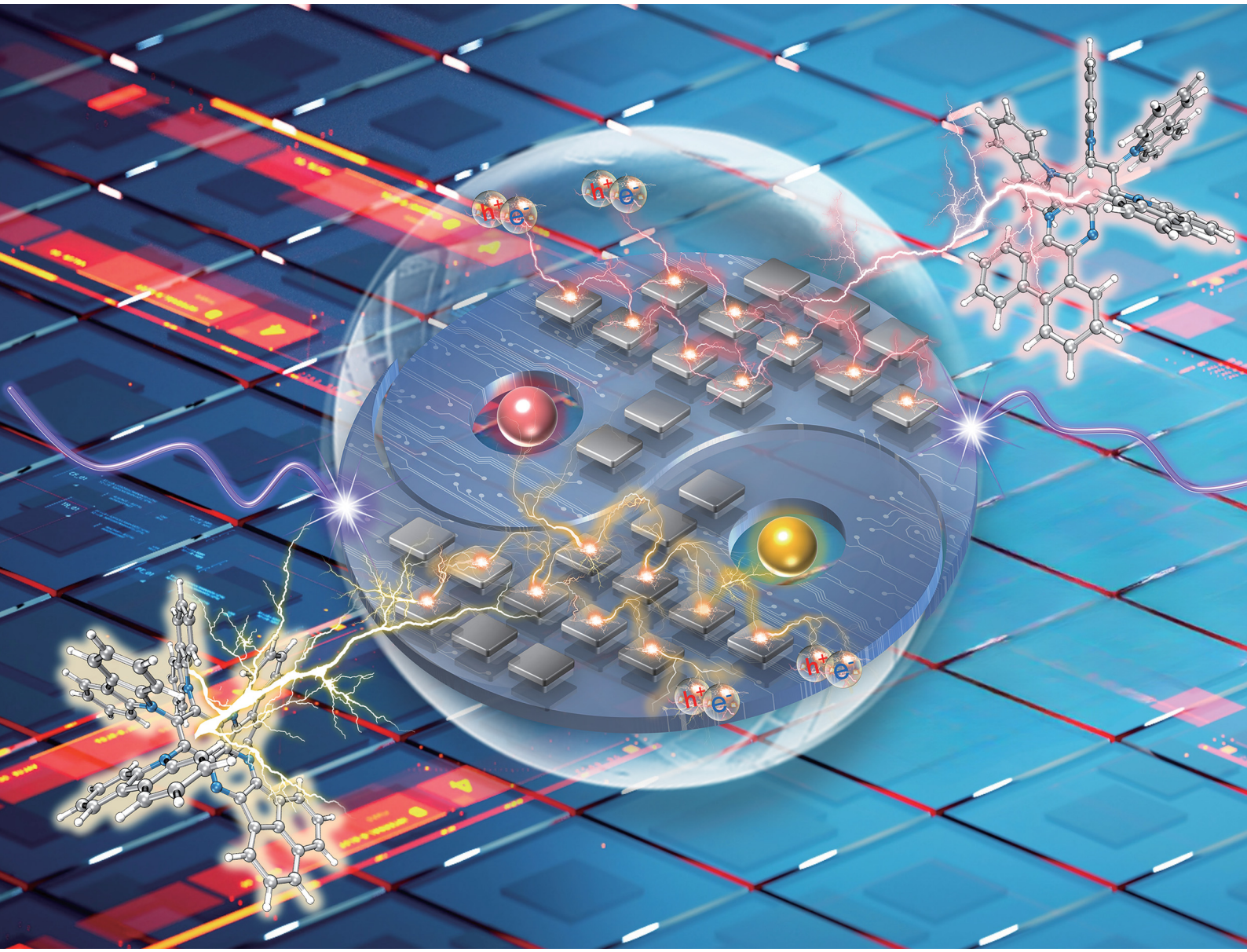

ISSN 2050-7526

ROYAL SOCIETY OF CHEMISTRY

PAPER

Wen-Cheng Chen, Hao-Li Zhang, Yanping Huo *et al.*
Efficient thermally activated delayed fluorophores featuring multi-donor arms and a π-extended acceptor core

Journal of Materials Chemistry C

ROYAL SOCIETY OF CHEMISTRY

PAPER

View Article Online
View Journal | View Issue

Cite this: J. Mater. Chem. C, 2024, 12, 6406

Efficient thermally activated delayed fluorophores featuring multi-donor arms and a π-extended acceptor core†

Bo Liu,[ab] Si-Wei Chen,[ab] Wen-Cheng Chen, *[ab] Longjiang Xing,[ab] Ji-Hua Tan,[ab] Wei-Le Wu,[ab] Xiao-Long Liu, [ab] Jia-Xiong Chen,[ab] Hao-Li Zhang *[c] and Yanping Huo *[abd]

Received 13th March 2024,
Accepted 13th April 2024

DOI: 10.1039/d4tc00988f

rsc.li/materials-c

Thermally activated delayed fluorophores often face challenges related to low solid-state luminescence efficiency and inefficient spin–flip processes, compromising their performances in organic light-emitting diodes. Herein, we introduce two new thermally activated delayed fluorophores, namely **4CzAQ** and **4CzDP**, based on a π-extended acceptor core (acenaphtho[1,2-*b*]quinoxaline/dibenzo[*a*,*c*]phenazine) and four electron-donating carbazolyl arms. These new emitters feature a propeller-like sterically demanding configuration, which mitigates emission quenching in the solid state. Crucially, this design strategy results in a dense charge-transfer excited-state alignment and strategically introduces locally excited triplet states from the acceptor within the alignment to facilitate spin flipping by a spin–vibronic coupling mechanism. The luminescence properties and spin-flipping efficiency can be finely tuned by varying the acceptor unit, depending on its π-conjugation extension and energy level. A device doped with 10 wt% of the optimal emitter, **4CzAQ**, achieves a remarkable electroluminescence performance with an external quantum efficiency of 26.8% and a peak at 555 nm. The combined steric and electronic modulation arising from this molecular design offers a compelling strategy to address critical challenges in thermally activated delayed fluorophores.

Introduction

Thermally activated delayed fluorescence (TADF) materials have drawn increasing attention and demonstrated their versatility in applications ranging from bioimaging,[1] sensing,[2] photocatalysis,[3] and lasers,[4] to optoelectronic devices.[5,6] Particularly, TADF compounds have become a subject of interest in the organic light-emitting diode (OLED) field, specifically for displays and lighting.[7,8] In contrast to conventional phosphors, TADF emitters stand out for their ability to fully utilize electrically formed singlet and triplet excitons without relying on noble metals,[9–11] highlighting their practical advantages, including notable efficiency, cost-effectiveness, and environmentally friendly nature. Despite blue and green TADF materials having been well developed, achieving comparable efficiencies in longer-wavelength TADF emitters remains a challenge because of the energy gap law,[12–14] resulting in increased non-radiative transition and lower luminescence efficiency.

Enhancing molecular rigidity is a proven method to diminish molecular rotation and vibration, consequently inhibiting non-radiative processes.[15] Thus, much effort has been devoted to developing new TADF materials with long-wavelength using π-extended rigid frameworks.[16–18] However, employment of extended π-conjugated motifs often leads to strong interchromophore interactions in the solid state, resulting in severe emission quenching and hindering electroluminescence (EL) performance improvement.[19] To mitigate emission quenching, the emissive materials must be dispersed within a suitable host material at low concentrations (<5 wt%).[20–22] Nevertheless, this method also brings about additional issues, such as insufficient host-to-guest energy transfer,[23] imbalanced charge

[a] Guangdong Provincial Laboratory of Chemistry and Fine Chemical Engineering Jieyang Center, Jieyang, 515200, P. R. China. E-mail: wencchen@gdut.edu.cn, yphuo@gdut.edu.cn
[b] School of Chemical Engineering and Light Industry, Guangdong University of Technology, Guangzhou, 510006, P. R. China
[c] State Key Laboratory of Applied Organic Chemistry (SKLAOC), Key Laboratory of Special Function Materials and Structure Design (MOE), College of Chemistry and Chemical Engineering, Lanzhou University, Lanzhou 730000, P. R. China. E-mail: haoli.zhang@lzu.edu.cn
[d] Analytical & Testing Center, Guangdong University of Technology, Guangzhou, 510006, P. R. China

† Electronic supplementary information (ESI) available: Experimental, characterization, photophysical data, and other additional information. CCDC 2224330 and 2224332. For ESI and crystallographic data in CIF or other electronic format see DOI: https://doi.org/10.1039/d4tc00988f

transport,[6] and the need for precise regulation of the evaporation rate during device fabrication.

Another approach to enhance the EL performance involves the promotion of reverse intersystem crossing (RISC). This compensates for excitons leaking through intersystem crossing (ISC), allowing more excitons to remain in the S_1 state, ready for fluorescence. Nevertheless, a typical twisted donor (D)–acceptor (A)-based TADF compound has a predominating charge transfer (CT) characterized S_1 and T_1 states (^{1}CT and ^{3}CT, respectively).[24,25] As per the EI-Sayed's rule, $^3CT \rightarrow {}^1CT$ spin flipping is theoretically forbidden as the spin–orbit coupling (SOC) matrix element between S_1 and T_1 with similar orbital features is extremely small.[26–28] This results in significant triplets accumulating at high excitation densities, leading to detrimental exciton losses.[29,30]

Theoretically, fine-tuning the D/A structure allows the placement of the locally excited (LE) triplet state of the donor (^3LE_D) or acceptor (^3LE_A) between or near ^{1}CT and ^{3}CT, promoting spin-flipping efficiency. As majority of the donors in twisted D–A-based TADF emitters are of limited conjugation with high ^3LE_D energy levels, modulating ^3LE_A is more practical for developing long-wavelength TADF emitters. Our previous research[14] and those of other groups[31–34] have underscored the crucial importance of the triplet energy level position of the acceptor component in achieving high efficiency in long-wavelength TADF systems. Besides, recent studies have indicated that introducing multiple donor moieties, typically carbazole derivatives, in TADF emitters significantly promotes their RISC rate constant (k_{RISC}).[35–37] This is attributed to the generation of charge-resonance hybrid triples and the emergence of a dense manifold of triplet states, offering rich spin-flipping channels through a second-order spin–vibronic coupling (SVC) mechanism.[38] Currently, most multi-carbazole-based TADF compounds rely on small-conjugated acceptors, such as benzonitrile[39–41] and triazine derivatives,[42–44] and achieving long-wavelength emission with EL peak of over 550 nm in this type of TADF system remains sporadic.[45,46]

In consideration of these insights, we propose that coupling multiple donors to a rigid, π-extended acceptor would be a potent strategy for creating high-performance long-wavelength TADF emitters. In this approach, the rigid, π-extended acceptor would provide a reasonably low-lying ^3LE_A that approaches the ^{1}CT and ^{3}CT manifolds to invoke the RISC process. Incorporating multi-donor units not only enriches the density of CT excited states, thereby further facilitating spin flipping through SVC-assisted RISC processes, but also acts as bulky protective arms to mitigate emission quenching. The proof-of-the-concept TADF emitters, namely 8,9,10,11-tetra(9*H*-carbazol-9-yl)acenaphtho[1,2-*b*]quinoxaline (**4CzAQ**) and 10,11,12,13-tetra(9*H*-carbazol-9-yl)dibenzo[*a*,*c*]phenazine (**4CzDP**), showcase long-wavelength emission of over 550 nm and mitigatory quenching behavior in the solid state. Furthermore, the new emitters showed decent k_{RISC} values of over 10^5 s^{-1}. Through a systematic structure–property relationship study, we observed that TADF properties can be finely tuned by adjusting the conjugation and electron-accepting capacity of the acceptor units, significantly influencing emission color and exciton dynamics. As a result, we obtained a high external quantum efficiency (EQE) of 26.8%, marking one of the highest efficiencies reported for multi-carbazole-based TADF OLEDs.

Wen-Cheng Chen

Wen-Cheng Chen is currently an associate professor in the School of Chemical Engineering and Light Industry at Guangdong University of Technology (GDUT) and concurrently holds a senior research position at the Guangdong Provincial Laboratory of Chemistry and Fine Chemical Engineering Jieyang Center. He received his doctoral degree in chemistry from City University of Hong Kong (CityU) in 2018 under the supervision of Prof. Chun-Sing Lee. Before joining GDUT, he worked as a senior research associate at the Center of Super-Diamond and Advanced Films (COSDAF) of CityU. His research interests are focused on the design and synthesis of organic luminescent materials for organic light-emitting diodes, anti-counterfeiting/encryption, and bioimaging.

Results and discussion

Synthesis and characterization

The chemical structures of the new TADF emitters, **4CzAQ** and **4CzDP**, are illustrated in Fig. 1. These molecules are characterized by a quadruple carbazole decoration combined with a π-extended acceptor core, composed of acenaphtho[1,2-*b*]quinoxaline (AQ) or dibenzo[*a*,*c*]phenazine (DP), respectively. The synthetic routes to **4CzAQ** and **4CzDP** are outlined in Scheme S1 (ESI†). Typically, synthesizing sterically demanding π-extended conjugated molecules presents challenges due to low coupling yields. To overcome this issue, the new multi-donor TADF emitters were synthesized through steric hindrance–insensitive nucleophilic aromatic substitution (SN_{Ar}) reactions[36] utilizing a multiply fluorinated π-extended pyrazine. This pyrazine can be readily obtained *via* the condensation reaction[47] of 3,4,5,6-tetrafluorobenzene-1,2-diamine and aromatic diketone.

4CzAQ and **4CzDP** were purified using temperature-gradient vacuum sublimation, followed by comprehensive characterization using NMR, mass spectroscopies, and crystallographic analyses. Their highest occupied molecular orbital (HOMO) energy levels (E_{HOMO}) were determined as −5.44 and −5.47 eV, respectively, based on the half-wave potentials from cyclic voltammetry curves (Fig. S1, ESI†). Additionally, the lowest unoccupied molecular orbital (LUMO) energy levels were calculated from $E_{HOMO} - E_g$ (optical energy gap estimated from the absorption onset) to be −2.92 and −3.15 eV, respectively. **4CzAQ** and **4CzDP** exhibit superior decomposition temperatures (5% weight loss) of 445.5 and 501.1 °C (Fig. S2 and Table S1, ESI†),

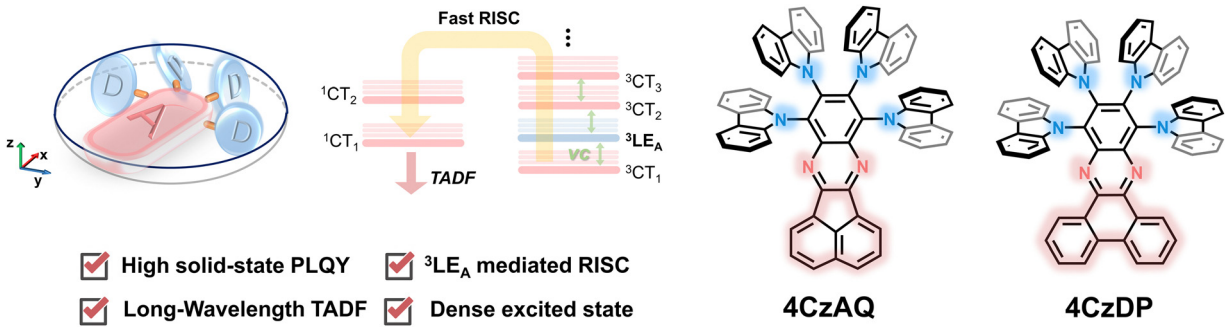

Fig. 1 The proposed molecular design for the long-wavelength TADF molecules with multi-donor arms and a π-extended acceptor core.

respectively, which are thermally stable for fabricating vacuum-deposited OLEDs.

Crystallographic analysis

The multi-donor cluster is believed to effectively shield the π-extended AQ and DP moieties from strong interchromophore interactions, thereby ensuring favorable solid-state luminescence properties. The influence of the quadruple carbazole decoration on molecular conformation and intermolecular interactions has been investigated through crystallographic analysis (Fig. 2). **4CzAQ** and **4CzDP** were initially dissolved in CH_2Cl_2 due to their relatively high solubility (>5 mg mL^{-1}), and then subjected to an anti-solvent (MeOH) vapor diffusion process to yield single crystals. Both new compounds exhibit a propeller-like bulky configuration, with D–A dihedral angles ranging from 53° to 67° (Fig. 2a). The densely packed carbazole motifs within the molecule can interlock with each other *via* steric hindrance and π interaction,[48] resulting in a stable conformation beneficial for suppressing non-radiative transitions.

It is observed that every two molecules of **4CzAQ** and **4CzDP** form an anti-symmetric head-to-head dimeric structure (Fig. 2b). This arrangement arises due to the less sterically demanding nature of the terminal part of AQ/DP (*i.e.*, the fused naphthyl and phenanthryl of AQ and DP, respectively). Due to DP's more extended π conjugation compared to AQ, intermolecular interactions become more pronounced, resulting in a shorter centroid–centroid distance between two adjacent AQ/DP units (Fig. 2b). Fortunately, the interchromophore interactions of both emitters are relatively weak, as evidenced by the limited intermolecular overlap (Fig. 2c), which helps preserve favorable solid-state luminescence, particularly for **4CzAQ**. Typically, reported multi-donor TADF emitters are based on acceptors with limited conjugation, often exhibiting a ball-like molecular configuration with minimal intermolecular contacts.[49] While this feature is desirable for maintaining

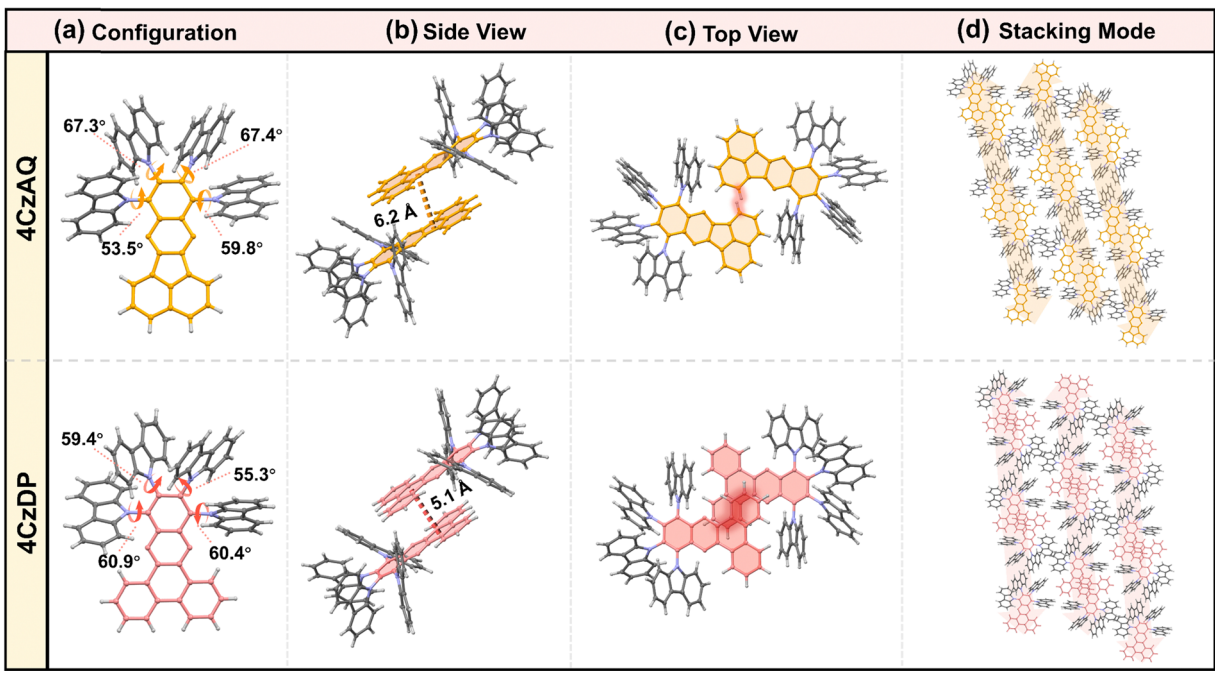

Fig. 2 Single crystal structures of **4CzAQ** and **4CzDP**: (a) configuration; the side view (b) and top view (c) of two molecular dimers; (d) single crystal stacking mode of two molecules.

excellent solid-state luminescence properties, it impedes carrier transport in solid film-based organic EL devices.[50] The present multi-carbazole decorated π-extended molecular design can overcome this trade-off by fostering suitable intermolecular contacts that facilitate a carrier hopping channel *via* π-extended acceptors (Fig. 2d).

Theoretical calculations

Theoretical calculations based on density functional theory (DFT) were performed to elucidate the electronic structures (Fig. 3 and Table S2, ESI†). Electrostatic potential mapping highlights the significance of the two sp^2-hybridized nitrogen atoms within the pyrazine segment as the primary electron-withdrawing components of AQ/DP, accentuated in red in Fig. 3a. Notably, in contrast to AQ, DP exhibits a larger extension of the red surface to its fused phenanthrene moiety, possibly due to its heightened degree of conjugation. This observation suggests DP's superior electron-accepting capabilities relative to AQ, as evidenced by its deeper LUMO level (−2.21 *vs.* −2.03 eV). Consequently, this results in stronger intramolecular charge transfer (ICT) and a narrower energy gap in **4CzDP** (Fig. 3b).

In general, most twisted D-A type TADF emitters exhibit near-zero oscillator strength (*f*) due to their perpendicular D–A structure, which results in compromised photoluminescence quantum yields (PLQYs), especially pronounced in long-wavelength emitters.[22] However, in our case, both **4CzAQ** and **4CzDP** demonstrate moderate-to-large D–A twisting angles just exceeding 60°. Although the HOMOs and LUMOs of **4CzAQ** and **4CzDP** mainly localize on the donor units and the π-extended acceptor, respectively, there is still discernible HOMO/LUMO overlap on the terminal fused benzene ring of the acceptors, resulting in the non-vanishing *f* values of 0.023 and 0.021 for **4CzAQ** and **4CzDP**. Furthermore, the nearly separated characteristics of the frontier molecular orbitals contribute to minimizing the exchange energy, resulting in reduced ΔE_{ST}s of 0.17 and 0.18 eV for **4CzAQ** and **4CzDP**, respectively.

Natural transition orbital (NTO) analyses were performed to gain insights into the excited-state characteristics of **4CzAQ** and **4CzDP**. As shown in Fig. 4, for the S_1 and T_1 states of both compounds, the holes and electrons are well distributed within the carbazole segments and the acceptor core, indicating a typical CT character of S_1 (^{1}CT) and T_1 states (^{3}CT). Other excited states, such as T_2, T_3, *etc.*, exhibit CT or hybridized local and charge-transfer (HLCT) characteristics featuring slightly different hole distribution patterns and are close in energy. Notably, the T_4 state of **4CzAQ** and the T_5 state of **4CzDP** exhibit features of LE character, with electron and hole density primarily localized on the acceptor unit, indicating they are ^3LE_A states. This is confirmed by their energy levels being equivalent to the T_1 state of the corresponding acceptor (Fig. S3, ESI†). Consequently, the ^3LE_A states are closely aligned in energy with the ^{1}CT and the dense ^{3}CT manifolds. In this scenario, despite the S_1 and T_1 excitations having comparable CT character, rendering direct SOC inefficient, the closely situated upper triplet excited states provide a viable RISC channel mediated by an SVC mechanism, in which the higher-order SOC for ^3LE_A–^{1}CT in thermal equilibrium plays a key role.[51] As a result, the SOC matrix element values of $\langle {}^1CT|\hat{H}_{SOC}|{}^3LE_A\rangle$ for **4CzAQ** ($^3LE_A = T_4$) and **4CzDP** ($^3LE_A = T_5$) are as high as 0.27 and 0.33 cm^{-1}, respectively, surpassing those of the corresponding $\langle S_1|\hat{H}_{SOC}|T_1\rangle$ (0.17 and 0.19 cm^{-1}).

Photophysical properties

Fig. 5a illustrates the UV-vis absorption and photoluminescence (PL) spectra in toluene (10^{-5} mol L^{-1}). The prominent absorption band observed below 370 nm is attributed to the π–π* transition of the carbazole and AQ/DP fragments. The bands

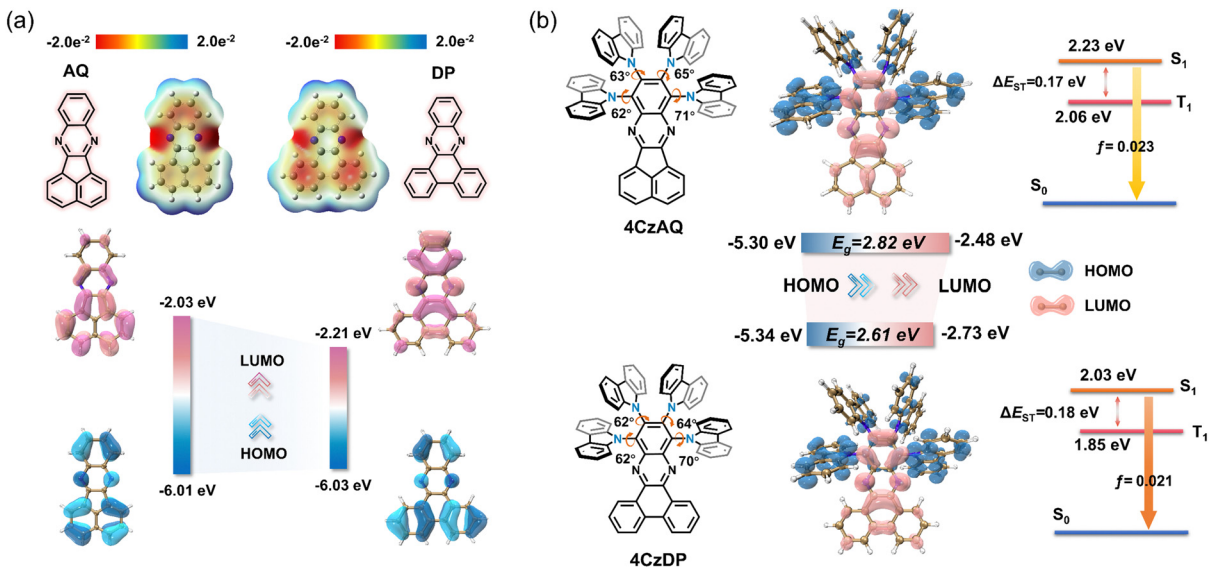

Fig. 3 (a) The electrostatic potential surfaces and HOMO/LUMO of AQ and DP. (b) Simulated optimized geometry, HOMO and LUMO distributions and single triplet energy level of **4CzAQ** and **4CzDP**.

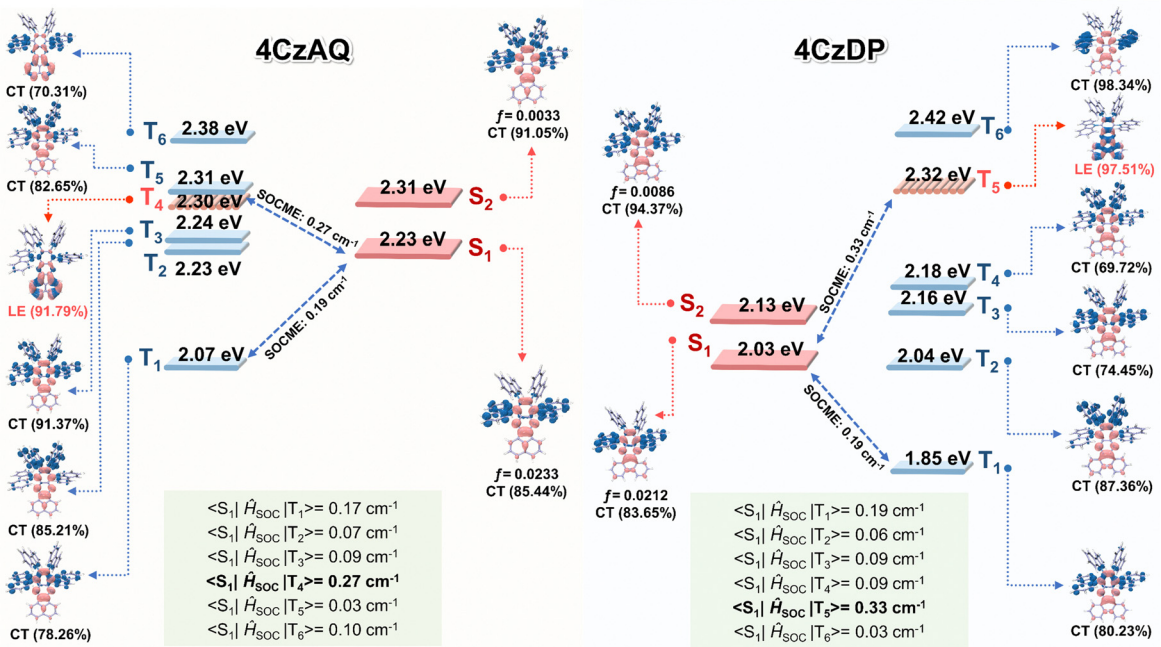

Fig. 4 Energy-level diagram with NTOs for the excited singlet (S_n) and triplet (T_m) states (Hole: blue color; particle: pink color), and SOC matrix elements between the T_m and S_n states of **4CzAQ** and **4CzDP**.

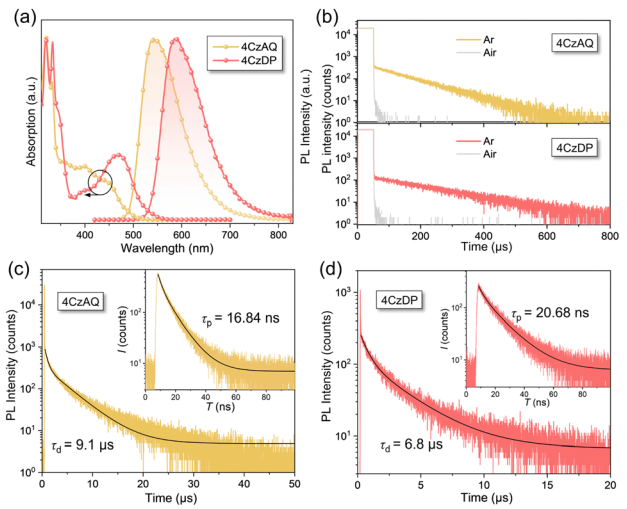

Fig. 5 (a) UV-vis absorption and PL spectra of **4CzAQ** and **4CzDP** in toluene (10^{-5} mol L^{-1}); (b) Transient PL decay curves of **4CzAQ** and **4CzDP** in toluene (10^{-5} mol L^{-1}) before and after Ar bubbling; (c) Transient PL decay curve of 10 wt% **4CzAQ**-doped CBP films at 300 K under a nitrogen atmosphere; (d) Transient PL decay curve of 10 wt% **4CzDP**-doped CBP films at 300 K under a nitrogen atmosphere.

with lower intensity ranging from 370 to 530 nm stem from the ICT transition. Notably, the ICT band of **4CzDP** is significantly stronger and redshifted compared to that of **4CzAQ**, consistent with the calculation results indicating DP's stronger acceptor character. Consequently, **4CzDP** exhibits longer-wavelength emission than **4CzAQ** (595 *vs.* 545 nm). Solvent-dependent PL spectra are presented in Fig. S4 (ESI†). The PL of both emitters undergoes distinct bathochromic shifts with increasing solvent polarity. In nonpolar *n*-hexane, the PL profiles of **4CzAQ** and **4CzDP** display delicate structures, gradually tuned to broader and featureless profiles in more polar solvents, indicative of typical ICT characteristics in excited states.[52]

We observed a distinct delayed component in the emission of both emitters after Ar bubbling, whereas the delayed fluorescence was completely quenched under air-equilibrated conditions (Fig. 5b), indicating the involvement of oxygen-sensitive triplet excitons. The PL decays of the two emitters comprise prompt fluorescence on a nanosecond scale and delayed fluorescence on a microsecond scale (Fig. 5c). The corresponding prompt (τ_{PF}) and delayed (τ_{DF}) lifetimes were fitted to be 16.84 ns/9.1 μs for **4CzAQ** and 20.68 ns/6.8 μs for **4CzDP**, respectively (Table 1). Furthermore, the contribution of delayed components increases with increasing temperatures (Fig. S5, ESI†), confirming the thermally accelerated RISC processes inherent in TADF.[45] The short τ_{DF} values for **4CzAQ** and **4CzDP** indicate a fast RISC process. However, due to the moderate D–A twisting angles, both in toluene and doped films, **4CzAQ** and **4CzDP** exhibit relatively large ΔE_{ST} values of 0.26/0.23 and 0.25/0.30 eV, respectively, as determined from the fluorescence and phosphorescence spectra (Fig. S6, ESI†). Combined with the theoretical calculations discussed above, it is envisioned that the ^3LE_A state may play a pivotal role in the RISC process.[53]

To verify this hypothesis, exciton dynamics were further investigated. First, the T_1 energy levels of carbazole, AQ, and DP were obtained from their phosphorescence spectra (Fig. 6a), and an energy level diagram of the new emitters and their components is plotted in Fig. 6b. It can be observed that the energy gap between the ^3LE_A and the S_1 of the corresponding

Table 1 Photophysical properties of **4CzAQ** and **4CzDP**

Emitter	λ_{abs}[a] (nm)	λ_{PL}[a] (nm)	τ_P[b] (ns)	τ_d[b] (μs)	E_{S1} (eV)	E_{T1} (eV)	ΔE_{ST} (eV)
4CzAQ	319/400	545	16.84	9.10	2.52[a]/2.46[b]	2.26[a]/2.23[b]	0.26[a]/0.23[b]
4CzDP	320/470	595	20.68	6.80	2.32[a]/2.34[b]	2.07[a]/2.04[b]	0.25[a]/0.30[b]

[a] Measured in toluene solution (10^{-5} mol L^{-1}). [b] Measured in 10 wt%-doped CBP films.

emitter is smaller than that of ΔE_{ST} (0.11 and 0.07 eV for **4CzAQ** and **4CzDP**, respectively), suggesting that ^3LE_A can serve as a potential mediator for spin flipping. Given carbazole's high T_1 energy level, ^3LE_D is unlikely to participate in the exciton RISC process. Next, the temperature dependencies of k_{ISC} and k_{RISC} were analyzed. The k_{RISC} rates as a function of temperature are plotted in Fig. 6c. The ISC and RISC activation energies (E_A^{ISC} and E_A^{RISC}) were obtained by linearly fitting the plots according to the Arrhenius dependence.[54,55] It was observed that while the E_A^{ISC} values of **4CzAQ** (6.8 meV) and **4CzDP** (7.2 meV) are nearly identical, the E_A^{RISC} values are quite different. Specifically, **4CzDP** exhibits a smaller E_A^{RISC} of 10.7 meV, notably smaller than that of **4CzDP** (21.1 meV). This disparity can be attributed to the smaller energy gap between ^3LE_A and S_1 of **4CzDP**. The lower E_A^{RISC} of **4CzDP** suggests a lower energy barrier for spin flipping. Consequently, **4CzDP** ($k_{RISC} = 1.57 \times 10^5$ s^{-1}) demonstrates a higher k_{RISC} than **4CzAQ** (1.37×10^5 s^{-1}). Thus, despite the relatively large ΔE_{ST} of the molecule, an efficient RISC process can be achieved by utilizing ^3LE_A as an accelerating intermediate.[56] This underscores the significance of the molecular design featuring a π-extended acceptor in a multi-donor TADF-type emitter.

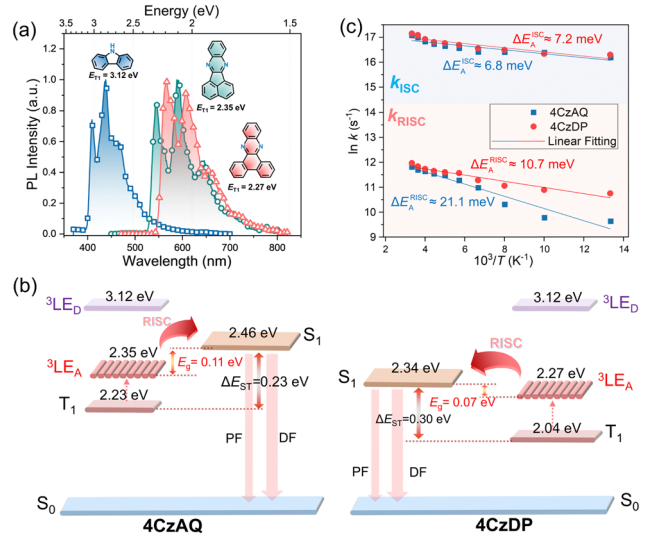

Fig. 6 (a) Phosphorescence spectra of AQ, PQ and carbazole (Cz) fragments with a delay of 10 ms at 77K; (b) temperature dependences of k_{ISC} and k_{RISC} for the 10 wt% TADF-emitter-doped CBP films (E_A is calculated according to the Arrhenius equation); (c) the schematic diagram of the exciton dynamic process of **4CzAQ** and **4CzDP**.

The solid-state photophysical properties were investigated with doped films in a 4,4'-bis(*N*-carbazolyl)-1,1'-biphenyl (CBP) host matrix. As illustrated in Fig. S7 (ESI†), with the increasing doping level from 5 to 50 wt%, the PL peak of the **4CzAQ** film exhibited a slight redshift from 535 to 554 nm (19 nm), while the shift for **4CzDP** was 31 nm (from 581 to 612 nm). Interestingly, compared to reported long-wavelength TADF emitters, **4CzAQ** demonstrates an insensitivity to doping concentration. The PLQY of the **4CzAQ** doped film (10 wt% in CBP) was estimated to be 92%, whereas that of **4CzDP** was only 58% (see Table 2). Notably, **4CzAQ** displays more obvious insensitivity than **4CzDP**, attributed to its loosely packed mode, which is conducive to achieving high EL performances.

Electroluminescence properties

To evaluate the EL performances of the proposed TADF compounds, a series of OLEDs were fabricated. The device structure comprised indium tin oxide (ITO)/2,3,6,7,10,11-hexacyano-1,4,5,8,9,12-hexaazatriphenylene (HAT-CN, 10 nm)/1,1-bis[(di-4-alkylamino)phenyl]cyclohexane (TAPC, 35 nm)/4,4′,4″tri(*N*-carbazolyl)-triphenylamine (TCTA, 10 nm)/1,3-bis(9*H*-carbazol-9-yl)benzene (mCP, 10 nm)/CBP: *x* wt% **4CzAQ** or **4CzDP** (20 nm)/1,3,5-tri[(3-pyridyl)-phen-3-yl]benzene (TmPyPB, 45 nm)/LiF (1 nm)/Al (*x* = 5, 10, 15, and 20). In this setup, ITO and Al were respectively utilized as the anode and cathode. HAT-CN acted as the hole-injection layer, TAPC as the hole-transporting layer, TCTA as the exciton-blocking layer, mCP as both the electron and exciton-blocking layer, and CBP as the hole-blocking layer. Furthermore, TmPyPB was employed as the electron-transporting layer, while LiF functioned as the electron injection layer. The efficiency calibration factors, obtained from the angular distribution of the EL intensity of the OLEDs (Fig. S8, ESI†), were 0.983 and 0.913 for **4CzAQ** and **4CzDP**, respectively.

As shown in Fig. S9 and Table S3 (ESI†), when the doping level increased from 5 to 20 wt%, the EL peak of **4CzAQ** experienced a redshift from 550 to 564 nm (14 nm), while that of **4CzDP** underwent a larger redshift from 594 to 616 nm (22 nm), consistent with the PL results (Fig. S7, ESI†). The EL performances of **4CzAQ** OLEDs improved with increased *x*,

Table 2 Physical properties of **4CzAQ** and **4CzDP** (10 wt% doped in CBP films)

Emitter	Φ_{PL} (%)	Φ_p (%)	Φ_d (%)	k_F ($\times 10^7$ s^{-1})	k_{ISC} ($\times 10^7$ s^{-1})	k_{RISC} ($\times 10^5$ s^{-1})	k_{nr} ($\times 10^7$ s^{-1})
4CzAQ	92	63	29	4.39	2.20	1.37	0.38
4CzDP	58	34	24	2.62	3.19	1.57	1.90

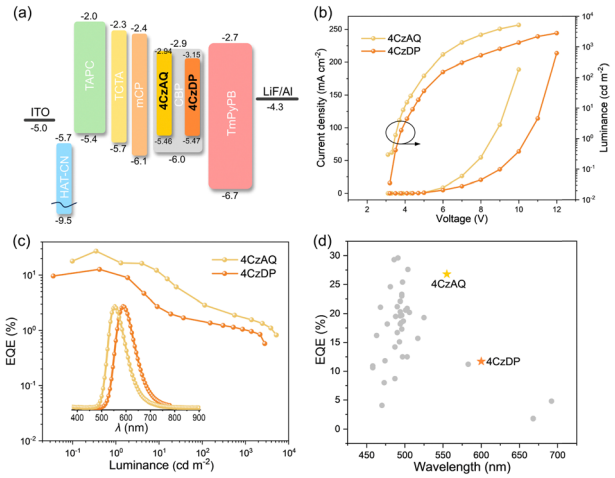

Fig. 7 (a) Device structures and energy level diagrams (unit: eV); (b) current density and luminance *versus* driving voltage characteristics (inset: Electroluminescence spectra at 100 cd m^{-2}) for **4CzAQ** and **4CzDP**; (c) external quantum efficiency *versus* luminance characteristics; (d) EQE_{max} comparison in terms of EL peaks with reported OLEDs based on multi-carbazole derivatives (references for the plotted data are given in Table S4, ESI†)

Table 3 EL performances of the devices based on **4CzAQ** and **4CzDP** (10 wt% doped in CBP)

Dopant	V_{on}[a] (V)	λ_{EL}[b] (nm)	CIE[c] (x, y)	CE_{max}[d] (cd A^{-1})	PE_{max}[e] (lm W^{-1})	EQE[f] (%)
4CzAQ	3.7	555	(0.43, 0.55)	60.5	57.5	26.8
4CzDP	3.8	600	(0.55, 0.44)	25.4	22.7	11.7

[a] Turn-on voltage at 1 cd m^{-2}. [b] EL peak wavelength at 100 cd m^{-2}. [c] CIE 1931 coordinates measured at 100 cd m^{-2}. [d] Maximum current efficiency. [e] Maximum power efficiency. [f] External quantum efficiency values at maximum.

reaching a maximum at x = 10. The 10 wt% doped **4CzAQ** OLED achieved a superior EQE_{max} of 26.8%, more than twice that of the **4CzDP** counterpart (11.7%), as shown in Fig. 7 and Table 3. Even under higher doping levels of 20 wt%, its EQE_{max} remained at a high level of over 17%. Conversely, although **4CzDP** exhibited a higher k_{RISC} than **4CzAQ**, it suffered from stronger interchromophore interactions, resulting in lower luminescence quantum efficiency, thereby compromising EL performances. The device performances of representative multi-carbazole TADF compounds are concisely summarized in Fig. 7d and Table S4 (ESI†). Remarkably, our new TADF materials demonstrate state-of-the-art EQE values,[57–59] particularly in the long-wavelength region with EL peaks exceeding 550 nm. These results affirm the efficacy of our molecular design tactics in constructing highly efficient long-wavelength TADF emitters.

Conclusion

In summary, this work presents two new TADF molecules, **4CzAQ** and **4CzDP**, developed through a strategic multi-donor coupled π-extended acceptor design. These materials are efficiently synthesized with decent yields and exhibit steric-demanding configurations that alleviate emission quenching, facilitating good luminescence efficiency. Notably, **4CzAQ** exhibits a higher PLQY of 92% due to its negligible interchromophore interaction. We reveal that the integration of the π-extended AQ/DP and carbazole units not only provides large molecular conjugation and intense ICT for long-wavelength emission with peaks of over 550 nm, but also offers a dense excited-state alignment with a ^3LE_A state as a crucial accelerating intermediate that facilitates RISC *via* the SVC mechanism. We also highlight the importance of the energy gap between the ^3LE_A and ^1CT states in tuning the rate of RISC; the smaller the gap, the lower the activation energy barrier for RISC. Because **4CzAQ** exhibits a superior PLQY and a relatively high k_{RISC}, its 10 wt% doped OLED showed a high EQE_{max} of 26.8% with an EL peak at 555 nm. The combined steric and electronic effects of the present molecular design provide an efficient approach for tackling challenges in long-wavelength TADF EL devices.

Conflicts of interest

The authors declare that they have no known competing financial interests or personal relationships that could have appeared to influence the work reported in this paper.

Acknowledgements

We sincerely acknowledge the financial support provided by the National Natural Science Foundation of China (Grant no. U2001222, U22A20399, U23A20594).

Notes and references

1 F. Fang, L. Zhu, M. Li, Y. Song, M. Sun, D. Zhao and J. Zhang, *Adv. Sci.*, 2021, **8**, 2102970.
2 X. Li, G. Baryshnikov, C. Deng, X. Bao, B. Wu, Y. Zhou, H. Ågren and L. Zhu, *Nat. Commun.*, 2019, **10**, 731.
3 M. A. Bryden and E. Zysman-Colman, *Chem. Soc. Rev.*, 2021, **50**, 7587–7680.
4 T. Zhang, Z. Zhou, X. Liu, K. Wang, Y. Fan, C. Zhang, J. Yao, Y. Yan and Y. S. Zhao, *J. Am. Chem. Soc.*, 2021, **143**, 20249–20255.
5 G. Chen, J. Wang, W.-C. Chen, Y. Gong, N. Zhuang, H. Liang, L. Xing, Y. Liu, S. Ji, H.-L. Zhang, Z. Zhao, Y. Huo and B. Z. Tang, *Adv. Funct. Mater.*, 2023, **33**, 2211893.
6 J.-H. Tan, J.-M. Jin, W.-C. Chen, C. Cao, R. Wang, Z.-L. Zhu, Y. Huo and C.-S. Lee, *ACS Appl. Mater. Interfaces*, 2022, **14**, 53120–53128.
7 R. Mac Ciarnáin, H. W. Mo, K. Nagayoshi, H. Fujimoto, K. Harada, R. Gehlhaar, T. H. Ke, P. Heremans and C. Adachi, *Adv. Mater.*, 2022, **34**, 2201409.
8 N. B. Kotadiya, P. W. M. Blom and G.-J. A. H. Wetzelaer, *Nat. Photonics*, 2019, **13**, 765–769.

9 S. O. Jeon, K. H. Lee, J. S. Kim, S.-G. Ihn, Y. S. Chung, J. W. Kim, H. Lee, S. Kim, H. Choi and J. Y. Lee, *Nat. Photonics*, 2021, **15**, 208–215.
10 Q. Liu, W.-C. Chen, R. Zhang, H. Wei, B. Liu, J.-M. Jin, Y. Liu, Z. Ye, J.-X. Chen, S. Ji, H.-L. Zhang and Y. Huo, *Dyes Pigm.*, 2023, **212**, 111125.
11 B. Liu, W.-C. Chen, R. Zhang, Q. Liu, H. Wei, W.-L. Wu, L. Xing, R. Wang, Y. Liu, S. Ji, H.-L. Zhang and Y. Huo, *Dyes Pigm.*, 2023, **216**, 111314.
12 R. Englman and J. Jortner, *Mol. Phys.*, 1970, **18**, 145–164.
13 Y. Xiao, H. Wang, Z. Xie, M. Shen, R. Huang, Y. Miao, G. Liu, T. Yu and W. Huang, *Chem. Sci.*, 2022, **13**, 8906–8923.
14 H. U. Kim, T. Kim, C. Kim, M. Kim and T. Park, *Adv. Funct. Mater.*, 2023, **33**, 2208082.
15 H.-Y. Zhang, H.-Y. Yang, M. Zhang, H. Lin, S.-L. Tao, C.-J. Zheng and X.-H. Zhang, *Mater. Horiz.*, 2022, **9**, 2425–2432.
16 H.-Y. Yang, H. Zhang, M. Zhang, X. Fan, H. Lin, S.-L. Tao, C.-J. Zheng and X.-H. Zhang, *Chem. Eng. J.*, 2022, **448**, 137717.
17 Y. Yuan, Y. Hu, Y.-X. Zhang, J.-D. Lin, Y.-K. Wang, Z.-Q. Jiang, L.-S. Liao and S.-T. Lee, *Adv. Funct. Mater.*, 2017, **27**, 1700986.
18 S. Wang, X. Yan, Z. Cheng, H. Zhang, Y. Liu and Y. Wang, *Angew. Chem., Int. Ed.*, 2015, **54**, 13068–13072.
19 H. Wang, J.-X. Chen, X.-C. Fan, Y.-C. Cheng, L. Zhou, X. Zhang, J. Yu, K. Wang and X.-H. Zhang, *ACS Appl. Mater. Interfaces*, 2023, **15**, 1685–1692.
20 U. Balijapalli, Y.-T. Lee, B. S. B. Karunathilaka, G. Tumen-Ulzii, M. Auffray, Y. Tsuchiya, H. Nakanotani and C. Adachi, *Angew. Chem., Int. Ed.*, 2021, **60**, 19364–19373.
21 J.-L. He, F.-C. Kong, B. Sun, X.-J. Wang, Q.-S. Tian, J. Fan and L.-S. Liao, *Chem. Eng. J.*, 2021, **424**, 130470.
22 J. Fan, J. Miao, N. Li, Y. Zeng, C. Ye, X. Yin and C. Yang, *J. Mater. Chem. C*, 2022, **10**, 10255–10261.
23 J. Pu, X. Nie, D. Li, X. Peng, W. Qiu, W. Li, D. Li, G. Sun, C. Shen, S. Ji, D. Cao and S.-J. Su, *Chem. Eng. J.*, 2023, **471**, 144508.
24 L. Zhou, H. Wang, Y.-Z. Shi, X.-C. Fan, J.-X. Chen, K. Wang, J. Yu and X.-H. Zhang, *Chem. Eng. J.*, 2022, **440**, 135775.
25 J.-X. Chen, H. Wang, Y.-F. Xiao, K. Wang, M.-H. Zheng, W.-C. Chen, L. Zhou, D. Hu, Y. Huo, C.-S. Lee and X.-H. Zhang, *Small*, 2022, **18**, 2201548.
26 M. A. El-Sayed, *J. Chem. Phys.*, 1963, **38**, 2834–2838.
27 Q. Zhang, H. Kuwabara, W. J. Potscavage, S. Huang, Y. Hatae, T. Shibata and C. Adachi, *J. Am. Chem. Soc.*, 2014, **136**, 18070–18081.
28 W. Zeng, T. Zhou, W. Ning, C. Zhong, J. He, S. Gong, G. Xie and C. Yang, *Adv. Mater.*, 2019, **31**, 1901404.
29 V. T. N. Mai, V. Ahmad, M. Mamada, T. Fukunaga, A. Shukla, J. Sobus, G. Krishnan, E. G. Moore, G. G. Andersson, C. Adachi, E. B. Namdas and S.-C. Lo, *Nat. Commun.*, 2020, **11**, 5623.
30 R. Chen, Y. Xu, Z. Zhou, H. Wang, Y. Jia, Q. Chang, P. Jin, B. Yin, C. Li and C. Zhang, *Phys. Rev. Appl.*, 2024, **21**, 014039.
31 J.-X. Chen, Y.-F. Xiao, K. Wang, D. Sun, X.-C. Fan, X. Zhang, M. Zhang, Y.-Z. Shi, J. Yu, F.-X. Geng, C.-S. Lee and X.-H. Zhang, *Angew. Chem., Int. Ed.*, 2021, **60**, 2478–2484.
32 S. Kothavale, W. J. Chung and J. Y. Lee, *J. Mater. Chem. C*, 2022, **10**, 6043–6049.
33 J. U. Kim, I. S. Park, C.-Y. Chan, M. Tanaka, Y. Tsuchiya, H. Nakanotani and C. Adachi, *Nat. Commun.*, 2020, **11**, 1765.
34 H. Lee, R. Braveenth, S. Muruganantham, C. Y. Jeon, H. S. Lee and J. H. Kwon, *Nat. Commun.*, 2023, **14**, 419.
35 H. S. Kim, J. Y. Lee, S. Shin, W. Jeong, S. H. Lee, S. Kim, J. Lee, M. C. Suh and S. Yoo, *Adv. Funct. Mater.*, 2021, **31**, 2104646.
36 L.-S. Cui, A. J. Gillett, S.-F. Zhang, H. Ye, Y. Liu, X.-K. Chen, Z.-S. Lin, E. W. Evans, W. K. Myers, T. K. Ronson, H. Nakanotani, S. Reineke, J.-L. Bredas, C. Adachi and R. H. Friend, *Nat. Photonics*, 2020, **14**, 636–642.
37 P. K. Samanta, D. Kim, V. Coropceanu and J.-L. Brédas, *J. Am. Chem. Soc.*, 2017, **139**, 4042–4051.
38 M. K. Etherington, J. Gibson, H. F. Higginbotham, T. J. Penfold and A. P. Monkman, *Nat. Commun.*, 2016, **7**, 13680.
39 D. Zhang, X. Song, A. J. Gillett, B. H. Drummond, S. T. E. Jones, G. Li, H. He, M. Cai, D. Credgington and L. Duan, *Adv. Mater.*, 2020, **32**, 1908355.
40 H. Noda, H. Nakanotani and C. Adachi, *Sci. Adv.*, 2018, **4**, eaao6910.
41 B. Madushani, M. Mamada, K. Goushi, T. B. Nguyen, H. Nakanotani, H. Kaji and C. Adachi, *Sci. Rep.*, 2023, **13**, 7644.
42 J.-R. Cha, C. W. Lee and M.-S. Gong, *Dyes Pigm.*, 2017, **140**, 399–406.
43 T. Matulaitis, P. Imbrasas, N. A. Kukhta, P. Baronas, T. Bučiūnas, D. Banevičius, K. Kazlauskas, J. V. Gražulevičius and S. Juršėnas, *J. Phys. Chem. C*, 2017, **121**, 23618–23625.
44 C. S. Oh, H. L. Lee, S. H. Han and J. Y. Lee, *Chem. – Eur. J.*, 2019, **25**, 642–648.
45 H. Uoyama, K. Goushi, K. Shizu, H. Nomura and C. Adachi, *Nature*, 2012, **492**, 234–238.
46 X. Zhou, Y. Xiang, S. Gong, Z. Chen, F. Ni, G. Xie and C. Yang, *Chem. Commun.*, 2019, **55**, 14190–14193.
47 X. Zhang, H. Wang, J.-X. Chen, L. Zhou, X.-Y. Hao, J. Yu, K. Wang and X.-H. Zhang, *Mater. Chem. Front.*, 2024, **8**, 1120–1127.
48 W.-C. Chen, M.-H. Zheng, Y.-L. Wu, R.-J. Wang, J.-M. Jin, S.-W. Chen, B. Liu, J.-X. Chen, Y. Huo and S. Ji, *Chem. Eng. J.*, 2024, **480**, 148314.
49 M. Mamada, H. Katagiri, C.-Y. Chan, Y.-T. Lee, K. Goushi, H. Nakanotani, T. Hatakeyama and C. Adachi, *Adv. Funct. Mater.*, 2022, **32**, 2204352.
50 W. Chen, Y. Yuan, G. Wu, H. Wei, L. Tang, Q. Tong, F. Wong and C. Lee, *Adv. Opt. Mater.*, 2014, **2**, 626–631.
51 H. L. Lee, J. Kang, J. Lim, S. C. Kim, S. O. Jeon and J. Y. Lee, *Nat. Commun.*, 2023, **14**, 4818.
52 Z. R. Grabowski, K. Rotkiewicz and W. Rettig, *Chem. Rev.*, 2003, **103**, 3899–4032.
53 T. Hosokai, H. Matsuzaki, H. Nakanotani, K. Tokumaru, T. Tsutsui, A. Furube, K. Nasu, H. Nomura, M. Yahiro and C. Adachi, *Sci. Adv.*, 2017, **3**, e1603282.
54 L. Skhirtladze, K. Lietonas, A. Bucinskas, D. Volyniuk, M. Mahmoudi, O. Mukbaniani, K. L. Woon, A. Ariffin

and J. V. Grazulevicius, *J. Mater. Chem. C*, 2022, **10**, 4929–4940.
55 T. Serevičius, R. Skaisgiris, I. Fiodorova, G. Kreiza, D. Banevičius, K. Kazlauskas, S. Tumkevičius and S. Juršėnas, *J. Mater. Chem. C*, 2021, **9**, 836–841.
56 H. Noda, X.-K. Chen, H. Nakanotani, T. Hosokai, M. Miyajima, N. Notsuka, Y. Kashima, J.-L. Brédas and C. Adachi, *Nat. Mater.*, 2019, **18**, 1084–1090.
57 F.-M. Xie, H.-Z. Li, K. Zhang, H.-Y. Wang, Y.-Q. Li and J.-X. Tang, *ACS Appl. Mater. Interfaces*, 2023, **15**, 39669–39676.
58 J. H. Yun, K. H. Lee, H. Jeong and J. Y. Lee, *J. Mater. Chem. C*, 2022, **10**, 10950–10956.
59 U. Balijapalli, M. Tanaka, M. Auffray, C.-Y. Chan, Y.-T. Lee, Y. Tsuchiya, H. Nakanotani and C. Adachi, *ACS Appl. Mater. Interfaces*, 2020, **12**, 9498–9506.